




RESEARCH PAPER

Biodegradable and Inherently Fluorescent pH-Responsive Nanoparticles for Cancer Drug Delivery

Kalindu Perera¹ · Dat X. Nguyen^{2,3} · Dingbowen Wang⁴ · Aneetta E. Kuriakose^{2,3} · Jian Yang⁴ · Kytai T. Nguyen^{2,3} · Jyothi U. Menon^{1,5} 

Received: 30 March 2022 / Accepted: 13 June 2022

© The Author(s), under exclusive licence to Springer Science+Business Media, LLC, part of Springer Nature 2022

Abstract

Purpose The development of two novel pH-only and pH- and thermo-responsive theranostic nanoparticle (NP) formulations to deliver an anticancer drug and track the accumulation and therapeutic efficacy of the formulations through inherent fluorescence.

Methods A pH-responsive formulation was synthesized from biodegradable photoluminescent polymer (BPLP) and sodium bicarbonate (SBC) via an emulsion technique, while a thermoresponsive BPLP copolymer (TFP) and SBC were used to synthesize a dual-stimuli responsive formulation via free radical co-polymerization. Cisplatin was employed as a model drug and encapsulated during synthesis. Size, surface charge, morphology, pH-dependent fluorescence, lower critical solution temperature (LCST; TFP NPs only), cytocompatibility and in vitro uptake, drug release kinetics and anticancer efficacy were assessed.

Results While all BPLP-SBC and TFP-SBC combinations produced spherical nanoparticles of a size between 200-300 nm, optimal polymer-SBC ratios were selected for further study. Of these, the optimal BPLP-SBC formulation was found to be cytocompatible against primary Type-1 alveolar epithelial cells (AT1) up to 100 µg/mL, and demonstrated sustained drug release over 14 days, dose-dependent uptake, and marked pH-dependent A549 cancer cell killing (72 vs. 24% cell viability, at pH 7.4 vs. 6.0). The optimal TFP-SBC formulation showed excellent cytocompatibility against AT1 cells up to 500 µg/mL, sustained release characteristics, dose-dependent uptake, pH-dependent (78% at pH 7.4 vs. 64% at pH 6.0 at 37°C) and marked temperature-dependent A549 cancer cell killing (64% at 37°C vs. 37% viability at pH 6.0, 41°C).

Conclusions In all, both formulations hold promise as inherently fluorescent, stimuli-responsive theranostic platforms for passively targeted anti-cancer therapy.

KEY WORDS fluorescent · nanoparticles · pH-sensitive · theranostic · thermoresponsive

Introduction

Cancer remains a major challenge in the field of medicine, particularly in developed nations. In the United States, all-cancer mortality was the second-leading cause of death, accounting for approximately 599,000 deaths in 2020, second only to cardiovascular disease (1). In clinical practice, chemotherapy remains one of the most common treatments to combat cancer, although acute toxicity (2), patient discomfort (2, 3), incomplete remission, development of multi-drug resistance (MDR) (4) and other drawbacks continue to plague these drugs. The development of stimuli-responsive drug delivery systems is one of a number of strategies that maximize chemotherapeutic efficacy while minimizing off-target effects. These systems can release their contents in

✉ Jyothi U. Menon
jmenon@uri.edu

¹ Department of Biomedical and Pharmaceutical Sciences, College of Pharmacy, University of Rhode Island, 7 Greenhouse Road, Kingston, Rhode Island 02881, USA

² Bioengineering Department, The University of Texas at Arlington, Arlington, Texas 76019, USA

³ Graduate Biomedical Engineering Program, The UT Southwestern Medical Center at Dallas, Dallas, Texas 75390, USA

⁴ Department of Biomedical Engineering, Pennsylvania State University, University Park, Pennsylvania 16802, USA

⁵ Department of Chemical Engineering, University of Rhode Island, Kingston, Rhode Island 02881, USA

response to changes in environmental stimuli- in this case, those observed within the tumor microenvironment.

The phenomenon of acidic tumor pH is one that has been well-characterized through the past decades. Driven primarily by the Warburg effect and tumor core hypoxia (both leading to excess lactic acid production) (5), the (extracellular) tumor microenvironment usually has a pH ranging between 5.5 and 7.4 (6). Numerous studies have taken advantage of the acidic tumor microenvironment to develop pH-dependent drug release or cell-targeting strategies for more effective treatment. Zhao *et al.* reported the development of pH-responsive polyethylene glycol-poly(lactide-co-glycolide) (PEG-PLGA) micelles using a tumor-specific pH-responsive peptide to effectively deliver paclitaxel to cancer cells and associated endothelial cells (7). These responsive polymeric micelles also showed *in vivo* anti-tumor activity against MCF-7 tumor-bearing mice. Kim *et al.* utilized biotin-based pH-responsive polymeric micelles to deliver doxorubicin to MCF-7 cells *in vitro* (8). They demonstrated the ability of biotinylated methoxypoly(ethylene glycol)-grafted-poly(β -amino ester) micelles to release significantly higher levels of doxorubicin than their non-biotinylated counterparts at acidic pHs. Work by Palanikumar *et al.* outlined an interesting method by which the acidic tumor microenvironment was exploited for enhanced uptake rather than triggered release (9). PLGA-based nanoparticles grafted with the acidity-triggered rational membrane (ATRAM) peptide were shown to be highly selective towards tumor regions and cancer cells in an acidic environment, with the ability to enter tumor cells in acidic environments relative to those at a neutral pH. These pH-responsive nanoparticle (NP) drug delivery platforms—whether triggered-release or direct targeting—could today be regarded as fundamental in cancer nanomedicine, on par with the nanoparticle size constraints demanded by the enhanced permeability and retention effects, a cornerstone of the field (10–12).

Theranostic nanoparticles are another development in the broader field of nanomedicine that has the potential to become a mainstay in cancer treatment. Imaging-enabled, drug-loaded nanoparticles have garnered attention in recent years as their accumulation within tumors can be tracked in real-time while providing localized treatment, all through a single platform (13). This approach requires the co-encapsulation of an imaging/contrast agent alongside a therapeutic one such that the accumulation of both at a target site serves as a measure of the platform's own efficacy. Fluorescent dyes, quantum dots (QDs), and superparamagnetic iron oxide nanoparticles (SPIONs) have been used in imaging-enabled nanoparticle systems due to such advantages as broad absorption spectra, high photostability, long luminescent lifetime, compatibility with magnetic guided imaging, or even the ability to deploy targeted hyperthermia (14, 15). However, both image-enabled QDs and SPIONs are known to exhibit notable off-target cellular injury via DNA damage and

oxidative stress (16–18), while fluorescent dyes suffer *in vivo* from poor bioavailability due to rapid clearance and/or poor solubility (limiting the window for imaging) and poor fluorescence quantum yield (resulting in poor contrast) (19). Furthermore, the incorporation of multiple components (i.e., imaging agents and therapeutic agents) within a single nanoparticle formulation leads to an increase in their hydrodynamic diameter, which can negatively impact their circulation half-life, as the rate of circulatory clearance has been observed to have a proportional relationship to the particle size (20). The development of nanoparticles using inherently fluorescent polymers has therefore become an attractive alternative in the field of theranostics.

This work describes the development of two types of stimuli-responsive photoluminescent nanoparticle systems for cancer treatment. One is a pH-responsive system utilizing a novel biodegradable photoluminescent polymer (BPLP) with sodium bicarbonate (SBC) called BPLP-SBC NPs, and the other comprises water-soluble BPLP, poly N-isopropylacrylamide (PNIPAm) and SBC to form a temperature- and pH-responsive system named TFP-SBC (thermoreponsive fluorescent particles-SBC) NPs. Both formulations (sans SBC) have previously been shown by us to be safe both *in vitro* and *in vivo* (21–23). Both nanoparticles (NPs) encapsulate the model drug cisplatin (cis), a platinum-containing anticancer drug that has been used as a first-line treatment for many types of cancers (24). BPLP itself is a relatively novel breakthrough in polymer synthesis by our group, possessing outstanding qualities suitable for tissue engineering applications, including excellent biocompatibility, biodegradability, high fluorescence yield, and photostability (21, 25). It has a demonstrated history of use in imaging-enabled, cancer-targeting nanoparticle applications to improve diagnostic accuracy without the need for organic dyes or quantum dots (23, 26, 27). PNIPAm is a well-known temperature-responsive polymer used extensively in drug delivery (28–30), while sodium bicarbonate (SBC, NaHCO_3) functions as a porogen in acidic environments by virtue of its rapid decomposition into CO_2 and water (31). The rapid release of CO_2 disrupts the polymeric shell of the NPs to facilitate the release of an encapsulated agent (31). Thus, the inclusion of SBC is a novel addition to extant BPLP-based technologies previously described in the literature and lends an additional layer of responsivity to the photo- and thermoresponsive polymers utilized. The fluorescent, stimuli-responsive nanoparticle systems developed herein are therefore presented as potential theranostics for cancer diagnosis and treatment.

Material and Methods

Materials

Biodegradable photoluminescent polymer (BPLP; 1200 Da) was synthesized following the protocol set out previously

(21). All chemicals were purchased from Sigma-Aldrich (St. Louis, MO) and used without modification unless specified. Cisplatin (Cayman Chemical, Ann Arbor, MI) and dialysis membrane (MWCO 1000 Da; Spectrum Labs, New Brunswick, NJ) were purchased and used as received. All cultured cell lines were obtained from the American Type Culture Collection (ATCC, Manassas, VA). Cell culture media and supplementary materials trypsin-EDTA, fetal bovine serum (FBS), and penicillin-streptomycin were purchased from Invitrogen Corp. (Carlsbad, CA).

Preparation of BPLP-SBC NPs

BPLP-SBC NPs were synthesized via a water-in-oil-in-water double emulsion, solvent-evaporation method (summarized on the right in Fig. 1). The first water phase was prepared by dissolving SBC in 1 mL de-ionized water. 10 mg of SBC was used for the synthesis of BPLP-(0.1)SBC particles, while 30 mg of SBC was used in BPLP-(0.3)SBC particle synthesis. Meanwhile, 120 mg of BPLP-Serine (BPLP-Ser)

was dissolved in 2 mL of 1,4-dioxane to establish the oil phase. The SBC solution was added dropwise into the BPLP solution while stirring at 400 rpm to form the primary emulsion. The resulting mixture was sonicated using an ultrasonic processor (Misonix Sonicators, Newtown, CT) at 30 W for 5 min and added to 25 mL of de-ionized (DI) water containing 400 mg of dissolved sodium dodecyl sulfate (SDS). This emulsion was sonicated at 30 W for 12 min in an ice bath to form the double emulsion. The resultant suspension was kept stirring for 6 h at room temperature (RT) to allow 1,4-dioxane evaporation. The BPLP-SBC emulsion was filtered using a 0.45 μm syringe filter (Fisher Sci, Fair Lawn, NJ) and dialyzed for 3 h using a 3500 Da (Da) molecular weight cut-off (MWCO) dialysis membrane. BPLP-SBC particles were finally obtained via lyophilization.

Preparation of TFP-SBC NPs

Since PNIPAm is soluble in water, a water-soluble form of BPLP was required for the synthesis of TFP-SBC NPs.

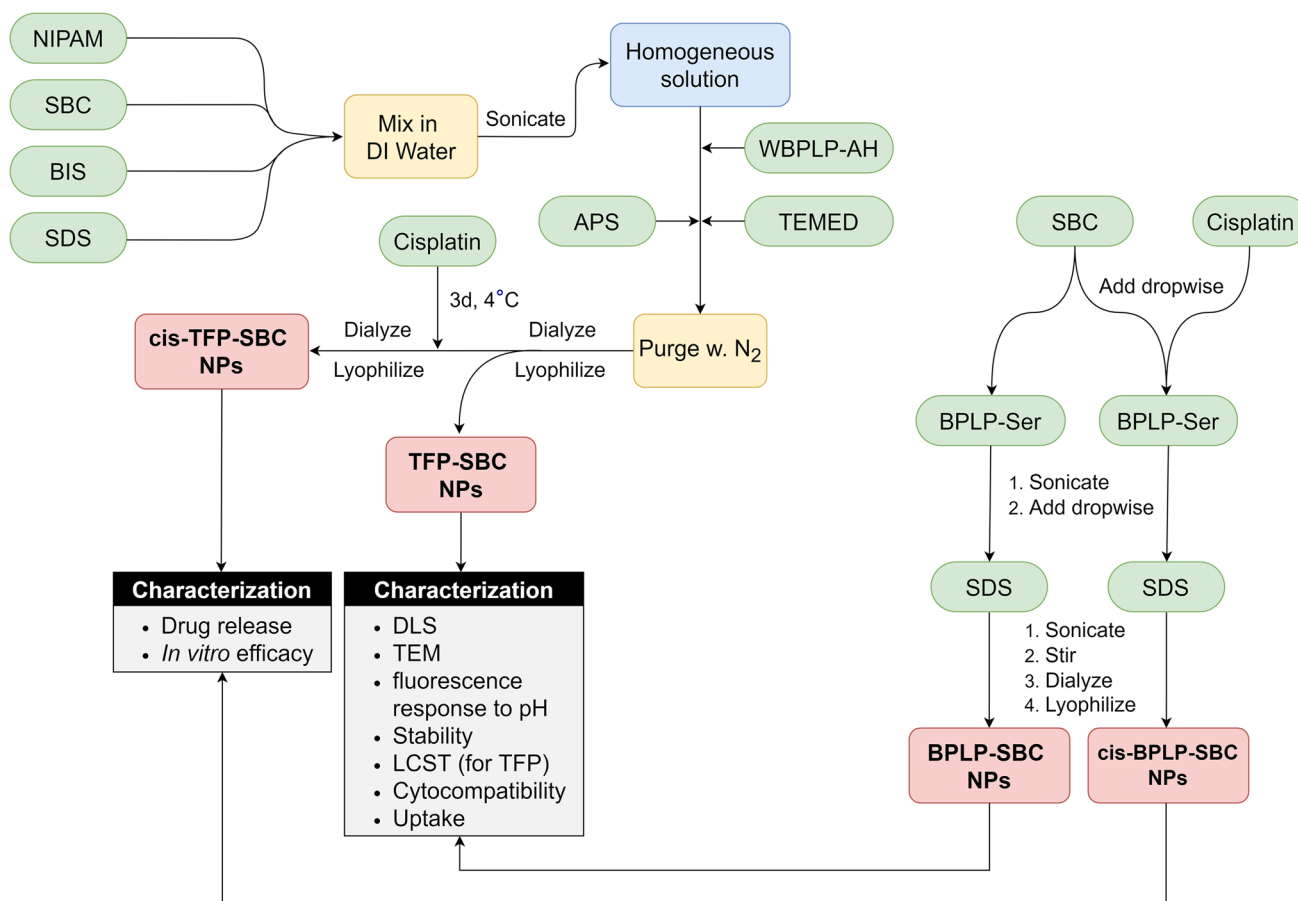


Fig. 1 Overview of the methodology followed, including synthesis, physical characterization, and *in vitro* characterization (NIPAM=N-isopropylacrylamide; SBC = sodium bicarbonate; BIS = N,N'-methylenebisacrylamide; SDS = sodium dodecyl sulfate; WBPLP-AH = water-soluble BPLP-allylamine crosslinked polymer; TEMED = tetramethylethylenediamine; APS = ammonium persulfate; BPLP = biodegradable photoluminescent particles; TFP = thermoresponsive fluorescent particles; ser = serine; cis = cisplatin; DLS = dynamic light scattering; TEM = transmission electron microscopy; LCST = lower critical solution temperature).

Accordingly, water-soluble BPLP-allylamine crosslinked polymer (WBPLP-AH; 1000 Da) was synthesized with the assistance of carbodiimide crosslinking chemistry. Specifically, 45 mg of WBPLP was dissolved in 5 mL of 2-(N-morpholino)ethanesulfonic acid (MES) buffer followed by the addition of 50 mg of N-(3-Dimethylaminopropyl)-N'-ethylcarbodiimide hydrochloride (EDC). This solution was subjected to mixing via rotary spinning for 30 min, after which 50 mg of N-hydroxysuccinimide (NHS) was added to it. After 1 h, 18.75 μ L of allylamine was added and mixed overnight. This was then filtered using a dialysis membrane for 24 h.

TFP-SBC nanoparticles using the prepared WBPLP-AH were synthesized via a free-radical polymerization method (summarized on the left in Fig. 1). In brief, 45 mg N-isopropylacrylamide (NIPAm; 113.16 Da), 5.85 mg N,N'-methylenebisacrylamide (BIS), 17.4 mg sodium dodecyl sulfate (SDS), and 10 mg (for TFP-(0.1)SBC) or 30 mg (for TFP-(0.3)SBC) sodium bicarbonate were added to 25 mL deionized water. The mixture was sonicated for 15 min at 30 W by an ultrasonic processor. 5 mL of WBPLP-AH (0.9% w/v) was then added to the sonicated mixture and purged with nitrogen for 15 min. Following this, 52.48 mg of ammonium persulfate (APS) and 69 μ L tetramethylethylenediamine (TEMED) were added to the purged solution to initiate and accelerate the polymerization process. This solution was kept stirring in a nitrogen atmosphere for 4 h before collection through 0.45 μ m syringe filtration. The product was dialyzed (MWCO 3500 Da) for 24 h to remove unreacted residue, followed by lyophilization to obtain the final TFP-SBC NPs.

Drug Loading

To prepare drug-loaded BPLP-SBC NPs (cis-BPLP-SBC NPs), cisplatin was dissolved in the W_1 phase alongside SBC during synthesis at a ratio of 1:5 with respect to polymer weight. Cis-TFP-SBC NPs were prepared by dissolving cisplatin in the same ratio as above in a suspension of TFP-SBC NPs in water. The resulting drug-particle suspension underwent rotary spinning for 3 days at 4°C to facilitate drug encapsulation in the thermosensitive polymer layer. The suspension was then subjected to dialysis (MWCO 1000 Da) for 4 h to remove any unloaded cisplatin. The dialysate was used for the calculation of loading efficiency. Lyophilization yielded the final cisplatin-loaded TFP-SBC NPs.

Nanoparticle Characterization

A 1 mg/mL sample of NPs (BPLP-(0.1)SBC, BPLP-(0.3)SBC, TFP-(0.1)SBC, TFP-(0.3)SBC) was examined for sizing, polydispersity index (PDI), and zeta potential using dynamic light scattering (Zeta PALS, Brookhaven

Instruments, NY). The same concentration of particles was used to obtain transmission electron microscope (TEM) images. A drop of the particle suspension was added to Formvar-coated 200-mesh copper grids (Electron Microscopy Sciences, Hartfield, PA) and allowed to air-dry, following which the sample was inserted into the TEM for imaging. The post-lyophilization stability of particles in 0.9% saline and media (10% serum) was assessed for up to 3 days *in vitro*, with samples being analyzed and kept in a 37°C incubator throughout.

Fluorescence intensity scans were carried out using an Infinite M200 microplate reader (Tecan, Switzerland). Particles were suspended in DI water at different pH values (3, 5, and 7.4) and underwent fluorescence intensity scanning with an excitation range of 380–700 nm and an emission range of 290–660 nm. Fluorescent visualization of NP suspensions was also carried out by suspending particles in de-ionized water of different pH (3 and 7.4) and placed in cuvettes under UV light for fluorescence images.

LCST Determination of TFP-SBC Nanoparticles

To characterize the thermoresponsivity of TFP-SBC nanoparticles, their LCST was determined by light capture via a photomultiplier (PMT). A 5 mg/mL suspension of TFP-SBC nanoparticles was prepared and placed in a quartz cuvette (Stama Cells, Atascadero, CA). The cuvette was placed in a water bath whose temperature was monitored using a temperature feedback probe. Laser light with a wavelength of 609 nm was directed at the sample, with the PMT capturing the scattered light at a 90° angle; a 594 nm long-pass filter was used to filter the captured light. The signal was captured 100 times on average, with the peak intensity of the emission decay curve being used to calculate light intensity. Results were plotted on a logarithmic scale of intensity units (A.U.) with respect to the temperature change of the suspension.

Assessment of AT1 Cytotoxicity

To evaluate the cytotoxicity of bare (drug-free) NPs on healthy cells, human alveolar type 1 (AT1) epithelial cells were used as a model cell line. These were seeded on 96-well plates at a density of 5×10^4 cells/well. Cells were cultured for 24 h before NP suspensions (in media) at various concentrations (0 to 500 μ g/mL) were added to the wells. After 4 h of incubation, the medium was removed and the cells were washed carefully with PBS, with fresh media added thereafter. MTS colorimetric assays were performed to determine cell viability, wherein 20 μ L of 3-(4,5-dimethylthiazol-2-yl)-5-(3-carboxymethoxyphenyl)-2-(4-sulfophenyl)-2H-tetrazolium (MTS) reagent (Promega, Madison, WI) was added to each well followed by 4 h incubation at 37°C. Results were obtained as absorbance readings at 490 nm using a microplate reader.

Evaluation of Drug Release

Drug release kinetics were evaluated for both nanoparticle formulations. In the case of BPLP-SBC NPs, this was carried out at two different pH values: 6.0 and 7.4. A 1 mg/mL concentration of cisplatin-loaded particles (cis-BPLP-SBC NPs) was transferred into a dialysis membrane with a MWCO of 3500 Da. The dialysis bags were then placed in water with the same pH as that of the drug-loaded particle suspension. At predetermined time points, 1 mL of the dialysate was collected and replaced with an equal volume of fresh dialysis media. Cumulative cisplatin release was analyzed by measuring the absorbance of collected dialysate samples at 300 nm and comparison with a cisplatin standard curve. For TFP-SBC NPs, cisplatin-loaded particles were assayed as above, at two different values of pH (6.0 and 7.4) and at two different temperatures (37° and 41°C).

Cellular Uptake and Uptake Imaging

A549 lung cancer cells were used as a model cancer cell line and seeded at a density of 2×10^5 cells/well on a 48-well plate. Cells were cultured for 24 h before NP suspensions (in media) at various concentrations (0 to 200 $\mu\text{g/mL}$) were added to the wells. After 2 h of incubation, the medium was removed, and the cells were washed carefully with PBS. The cells were fixed using 500 μL of 4% paraformaldehyde in PBS per well and kept at RT for 30 min. Paraformaldehyde was aspirated and replaced with fresh PBS, after which imaging was carried out using a Nikon Eclipse Ti microscope. The fluorescence intensity of images was quantified using the ImageJ software (32).

Assessment of *In Vitro* Therapeutic Efficacy

A549 lung cancer cells were seeded and incubated in 96-well plates at 37°C and 41°C one day prior to the experiment. Four distinct test groups were employed to assess the therapeutic efficacy of the nanoparticles here synthesized: control, free drug, bare NPs, and cisplatin-loaded NPs, in media at two different pH (6.0 and 7.4; for BPLP- and TFP-based NPs) and at two different temperatures (37° and 41°C; for TFP-based NPs only). Particle concentrations to be used were determined via IC₅₀ values of cisplatin against A549 cells (IC₅₀ 64 μM (33)) and known drug loading efficiencies of the NP batches used. Therefore, 250 $\mu\text{g/mL}$ BPLP-SBC NPs and 225 $\mu\text{g/mL}$ TFP-SBC NPs were used in the studies to release approx. 64 μM cisplatin within 24 h. Following the addition of NP suspensions in media at the appropriate pH, the cells were incubated at either 37°C or 41°C for 24 h. Media from each well was then aspirated, stored, and replaced with fresh media, followed by the addition of MTS reagents. Following incubation, absorbance readings

at 490 nm were collected using an Infinite M200 microplate reader. A parallel LDH cytotoxicity assay was also performed. Stored media from each well was centrifuged to collect the supernatant, and 100 μL of LDH working solution (Promega, Madison, WI)—prepared per manufacturer's instructions—was added to an equal volume of supernatant. After 30 min at RT, absorbance readings at 490 nm were collected using the microplate reader.

Results and Discussion

Nanoparticle Synthesis and Characterization

In this work, we synthesized NPs using two different methods: double emulsion for BPLP-SBC NPs and free radical copolymerization for TFP-SBC NPs, as outlined previously. These inherently fluorescent nanoparticles were lyophilized, wrapped in aluminum foil to protect from light, and stored at -20°C until required.

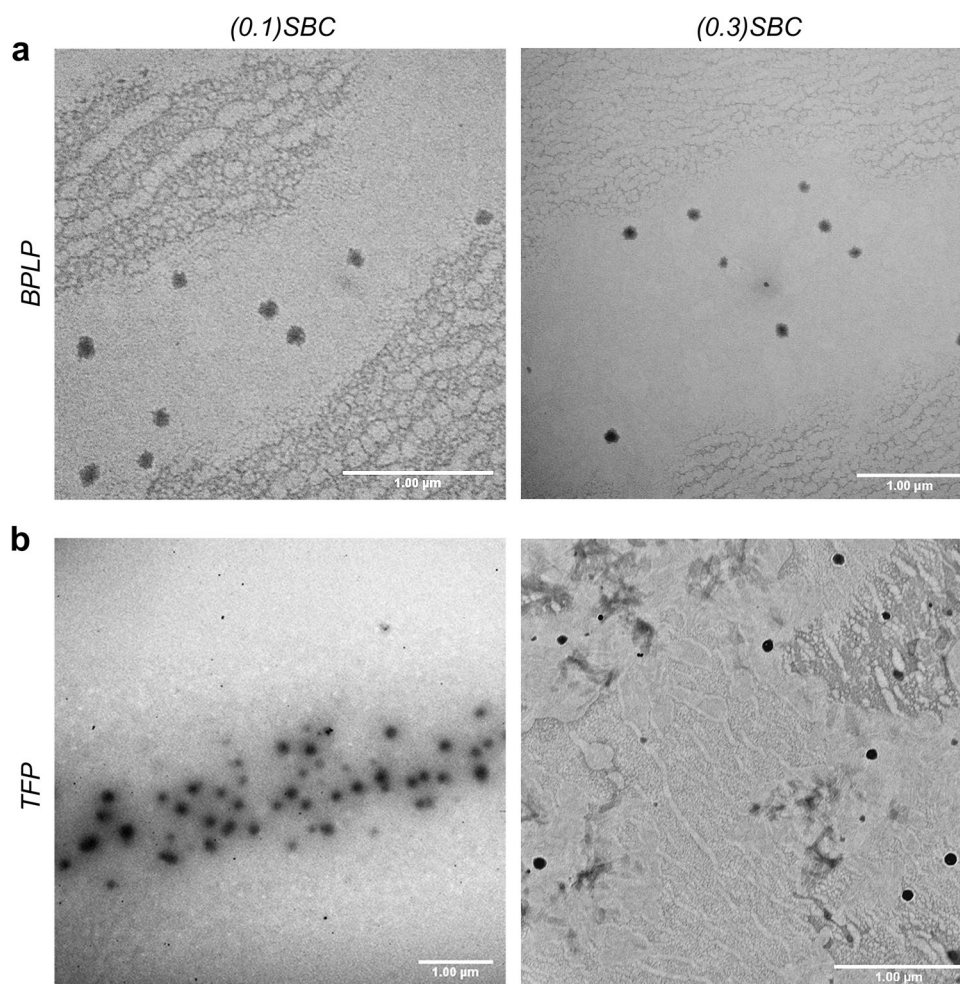
DLS data, including (hydrodynamic) particle size, polydispersity index (PDI), and surface charge of the synthesized NPs are presented in Table I (DLS data of nanoparticles not incorporated with SBC are presented in the Supporting Information, Table S-I). Overall, higher concentrations of SBC resulted in larger particle sizes as measured by both DLS and TEM, a trend previously observed (34). BPLP-(0.1)SBC NPs were observed to have a hydrodynamic diameter of 226 ± 7 nm while the (0.3)SBC counterpart was slightly larger, at 249 ± 7 nm. The same trend held true for the two TFP-based formulations: 298 ± 40 nm for (0.1) SBC and 340 ± 16 nm for (0.3)SBC NPs. BPLP NPs were of a smaller size than their TFP counterparts, with the former also possessing lower PDI values. Zeta potential values ranged from -34.4 to -27.5 mV for BPLP-SBC and from -19.7 to -19.2 mV for TFP-SBC, corresponding to the effect of anionic SDS surfactant coating on the surface of the particles. The latter can therefore be identified to be more unstable in suspension than the former. These sizes and zeta potentials agree with—or closely match—values observed previously by other groups and us (26, 27, 35).

TEM analysis of the nanoparticles showed BPLP-SBC NPs possessed a diffuse, near-spherical morphology. As

Table I DLS/zeta Potentiometry Data for Synthesized SBC-Incorporated Nanoparticle Formulations (Data from Measurements Done in Triplicates)

Sample	Size (nm)	PDI	Zeta potential (mV)
BPLP-(0.1)SBC	226 ± 7	0.256 ± 0.03	-34.4 ± 2.37
BPLP-(0.3)SBC	249 ± 7	0.224 ± 0.058	-27.5 ± 4.25
TFP-(0.1)SBC	298 ± 40	0.332 ± 0.027	-19.7 ± 2.82
TFP-(0.3)SBC	340 ± 16	0.300 ± 0.039	-19.2 ± 1.26

Fig. 2 Transmission electron micrographs of: (a) BPLP-SBC NPs (left: 0.1 M SBC, right: 0.3 M SBC) and (b) TFP-SBC NPs (left: 0.1 M SBC, right: 0.3 M SBC). Note the wider variation in particle size in the TFP samples, and the more diffused morphology of the BPLP NPs (Scale bar = 1 μ m).



shown in Fig. 2a, the (0.1)SBC NPs possessed a mean size of 113 ± 18 nm, and the (0.3)SBC NPs were slightly smaller at 105 ± 15 nm. TFP-SBC NPs (Fig. 2b) possessed a spherical morphology, albeit with a wider size range: the (0.1)SBC NPs possessed a mean size of 109 ± 29 nm, and the (0.3) SBC NPs were considerably smaller at 75 ± 14 nm. In both formulations, the same trend in size differentials between the 0.1 and 0.3 formulations of each type observed using DLS was apparent in TEM measurements as well. The difference in particle size between the DLS and TEM is attributed to the former's measurement of a larger, hydrodynamic diameter while the latter measures air-dried samples on a copper grid. Nevertheless, the BPLP-SBC NPs possessing a lower PDI/narrower size distribution relative to TFP-SBC NPs could possibly be attributed to the incorporation of the second polymer (PNIPAm) in the latter, leading to larger diameters.

The choice of SBC as a porogen was based on various factors, including data from previous work carried out by us (34, 36). For one, more traditional porogen such as poly(acrylic acid), Pluronic or ammonium bicarbonate suffer from non-ideal physicochemical properties, high cost, or

the need for steps such as thermal curing (37–39). SBC, in contrast, is a low-cost alternative that provides porogenic activity by simple salt leaching without the need for expensive and/or harsh leaching agents. Secondly, our previous work has shown that SBC tends to produce larger, more interconnected pore networks within particles: a much-desired characteristic allowing for rapid and efficient release of encapsulated payloads (36). There is, however, a limit to the amount of SBC that is compatible with the successful formation of BPLP or TFP nanoparticles: although we have attempted to synthesize particles with as much as 60 mg SBC (data not shown), these efforts were not successful, limiting us to the 30 mg utilized herein.

A major premise of the theranostic platforms here described is the ability of the NPs to provide fluorescence signals and thus help diagnose and track the efficacy of treatment within tumor-afflicted tissues/organs. Ideally, the NPs should either fluoresce stronger at the acidic pH in the lactic acid-rich tumor microenvironment or fluoresce at least as strongly as they do at normal physiological pH. To assess this characteristic in the synthesized NPs, their fluorescence spectra in solutions of different pH values were collected,

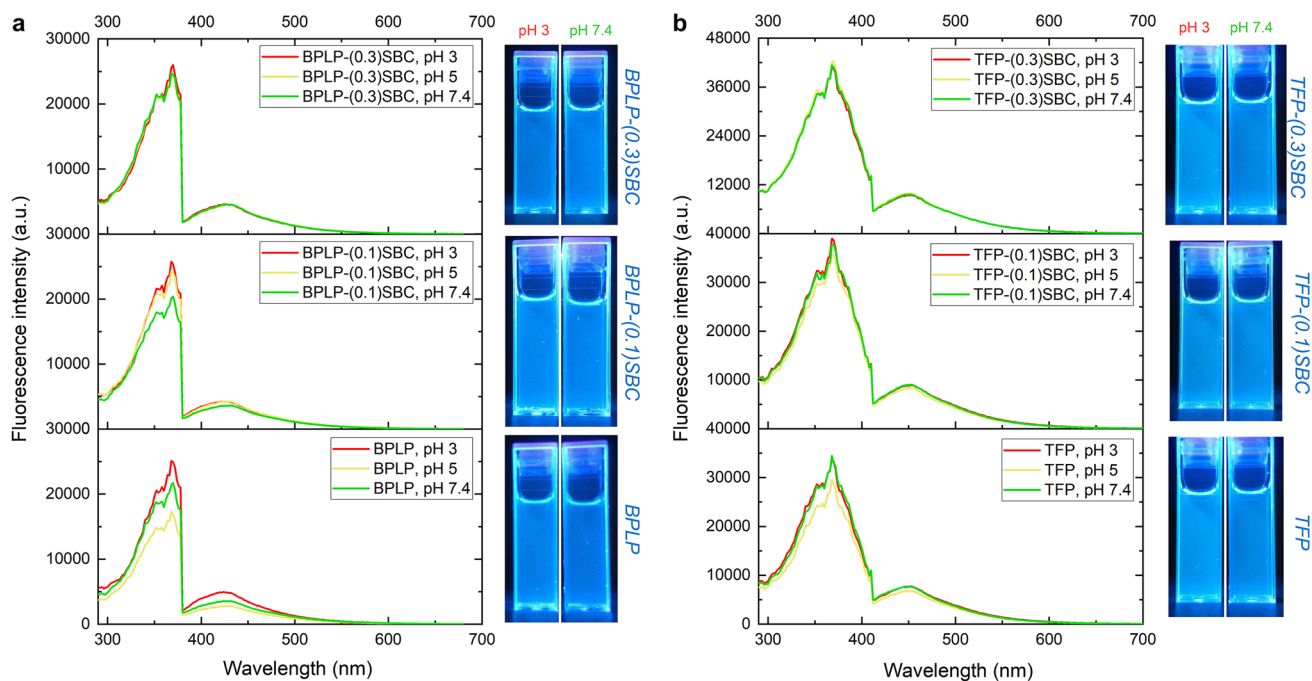


Fig. 3 Fluorescence intensity scans of **(a)** BPLP and BPLP-SBC NPs and **(b)** TFP and TFP-SBC NPs at various pH values at a 380–700 nm excitation range and 290–660 nm emission range. **(a)** also presents fluorescent images of BPLP-based NPs captured under UV light, while **(b)** presents corresponding images of the TFP-based particles.

and are shown in Fig. 3. All formulations (apart from BPLP on its own) showed either higher or similar intensities at acidic pH relative to neutral pH (with emission wavelengths seen previously in these formulations) (21). TFP-based NPs, in particular (Fig. 3b), showed almost no appreciable difference in intensity at the three pH values. These findings suggest that variations of pH or the concentrations of SBC used do not significantly affect the fluorescence intensity of the particles.

Figure 3 also presents photos of the NPs captured under UV light for comparison, which confirm negligible changes in fluorescence intensity amongst the different formulations and pH values. Comparison of the UV fluorescence of base BPLP- and TFP NP suspensions with deionized water controls and the appearance of TFP-based NP suspensions under visible light are presented in the Supporting Information (Fig. S1).

The stability of the synthesized NPs is also key to their success *in vivo* application; previous studies had successfully administered BPLP-based particles through an intravenous application (23). This is also envisioned for the particles developed herein, resulting in these particles spending an appreciable length of time circulating in the blood. As such, their stability in 0.9% saline and culture medium (containing 10% serum) were assessed- this data is presented in Fig. 4. BPLP-based NPs (Fig. 4a) stayed within approximately 20% of their initial diameter, with those in culture media being very stable and those in the salt solutions undergoing

a minor decrease in size after 24 h, after which the size remained constant for the duration of the study. By contrast, while TFP-based NPs (Fig. 4b) stayed stable in culture media, those in the salt solutions showed marked swelling up to approximately 40% of day 0 size. This is most likely a result of the incorporation of PNIPAm in their structure: the polymer has a documented propensity to swell in saline solutions (40, 41). Overall, all formulations remained within 40% of day 0 size, indicating no major problems with stability in suspension.

LCST Determination of TFP-SBC Nanoparticles

A fundamental principle behind the function of the TFP-based NPs is their ability to undergo a reversible phase transition and to swell or shrink in order to release their encapsulated payload. This ability was assessed by way of the lower critical solution temperature (LCST) of the NPs in solutions of two different pH. This data is presented in Fig. 5 and demonstrates that the LCST of TFP-(0.1) SBC and TFP-(0.3) SBC NPs at pH 7.4 are 38.6°C and 49.9°C, respectively. At a lower pH of 6, the LCST of both formulations decreased slightly (TFP-(0.1) SBC to 38.4°C and TFP-(0.3)SBC to 45.4°C). This is a previously-documented phenomenon, wherein the hydrogen bonding within the PNIPAm hydrogel is disrupted as the environment gets more strongly acidic/alkaline, leading to partial ionization of the hydrogel network and an easier path to phase transition (42). The phase

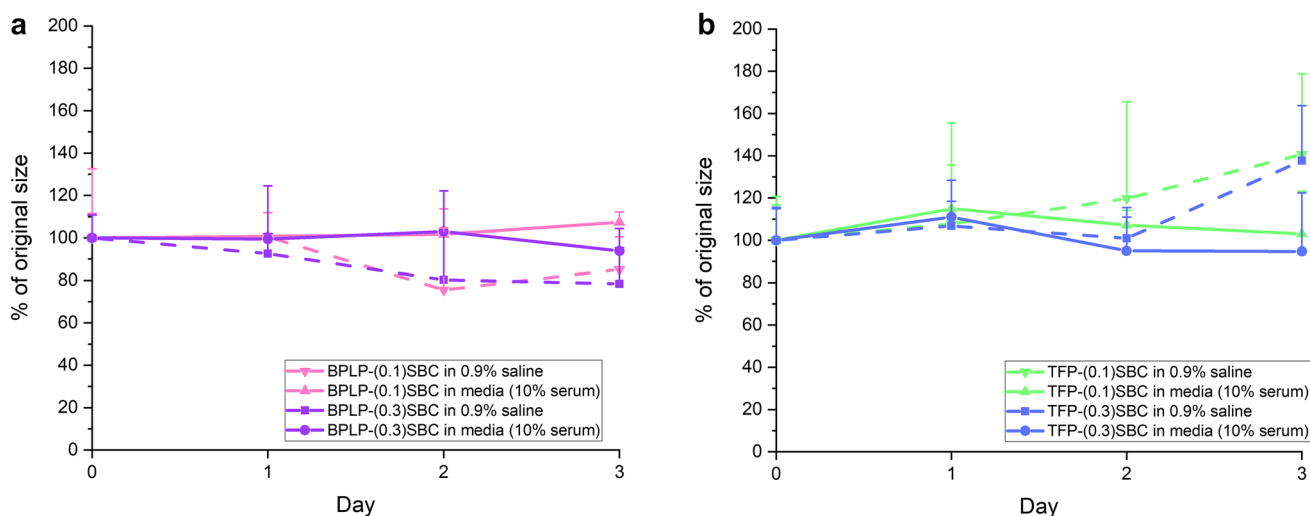


Fig. 4 Functional capacity testing data for the two nanoformulations. (a) Stability of BPLP-SBC NPs in 0.9% saline and media (with 10% serum) over a 3-day period. (b) Corresponding stability data for TFP-SBC NPs. Note the slight swelling of these particles in the saline solution.

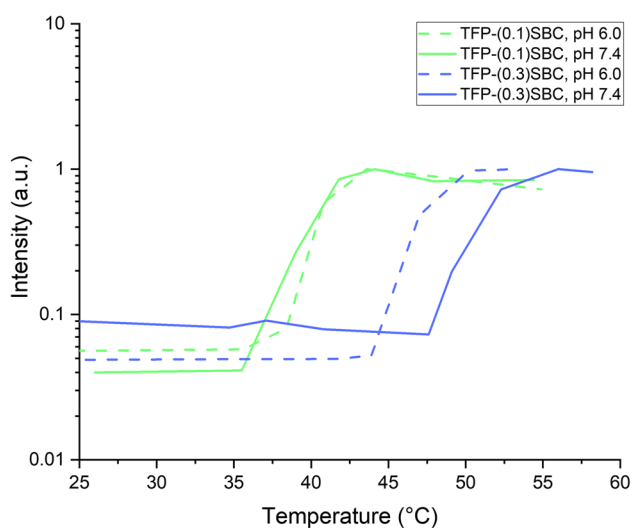


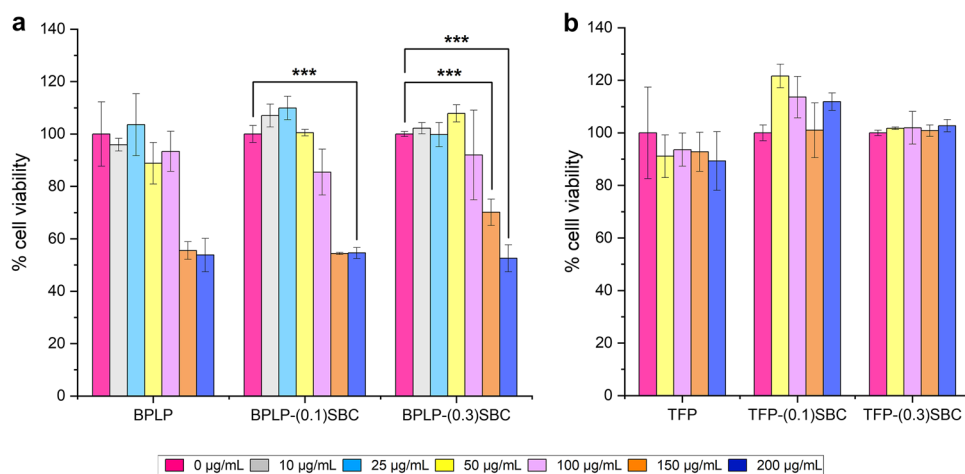
Fig. 5 Data indicative of lower critical solution temperature (LCST) of TFP NPs in solutions with different pH, determined via fluorescence intensity scanning.

transition was also clearly observable visually, with the NP suspensions turning from transparent to translucent at temperatures above their respective LCSTs, a distinctive sign of this transition (43). Images of TFP NPs pre- and post-LCST are presented in the Supporting Information (Fig. S2).

Assessment of AT1 Cytotoxicity

The cytocompatibility of all BPLP- and TFP-based NPs were determined by the incubation of a range of NP concentrations with AT1 cells for 24 h, up to a maximum of 200 $\mu\text{g}/\text{mL}$. Results (Fig. 6a) showed that BPLP and BPLP-SBC NPs remained cytocompatible ($\geq 80\%$ viability) towards AT1 cells at up to 100 $\mu\text{g}/\text{mL}$, with signs of cell death appearing at 150 $\mu\text{g}/\text{mL}$ and persisting at 200 $\mu\text{g}/\text{mL}$. At 200 $\mu\text{g}/\text{mL}$, all BPLP-based NPs caused a reduction in viability to approximately 55%. BPLP-based NPs were thus confirmed to be cytocompatible against AT1 cells at concentrations up to 100 $\mu\text{g}/\text{mL}$. Interestingly,

Fig. 6 Evaluation of cytocompatibility (relative to control) of (a) BPLP-based NPs, and (b) TFP-based NPs using the MTS assay on AT1 cells after 24 h exposure. While the former showed cytocompatibility up to 100 $\mu\text{g}/\text{mL}$, the latter showed only minor decreases in cytocompatibility up to the maximum concentration of particles tested. ($n=3$ for all groups; *** $p \leq 0.001$).



this phenomenon of BPLP NP toxicity at concentrations of $>100 \mu\text{g/mL}$ has not been reported previously in the available literature. This is, however, the first instance of these nanoparticles being tested for cytocompatibility against AT1 cells, and this data may serve as a valuable addition to the existing knowledge base on BPLP. Previous work with BPLP-based NPs has looked at their cytocompatibility with human dermal fibroblasts (HDFs) (22, 23, 26), THP-1 (35), WM35 (35), 1205Lu (35), PZ-HPV-7 (23) and HUVECs (22). Magnetic BPLP NPs were found to be cytocompatible up to $200 \mu\text{g/mL}$ at 72 h against HDFs (22). Muramyl-tripeptide-linked BPLP NPs caused no cytotoxicity towards THP-1 cells after 24 h at concentrations up to $1000 \mu\text{g/mL}$, some cytotoxicity towards WM35 cells after 24 h at $1000 \mu\text{g/mL}$, and cytotoxicity to 1205Lu cells after 24 h at $500 \mu\text{g/mL}$ (35). HUVECs experienced no cytotoxicity at concentrations up to $1000 \mu\text{g/mL}$ after 24 h (26). AT1 cells are known to be very sensitive to damage in general compared to other cells in the lungs, so the marked difference in cytotoxicity when exposed to these nanoparticles is to be expected (44, 45).

TFP, TFP-(0.1)SBC, and TFP-(0.3)SBC NPs showed acceptable levels of cytocompatibility ($\geq 80\%$ viability; Fig. 6b) up to a concentration of $200 \mu\text{g/mL}$ (and beyond to $500 \mu\text{g/mL}$; see Supporting Information Fig. S3). Even at $500 \mu\text{g/mL}$, TFP particles were shown to affect AT1 by decreasing cell viability to only 82%, while neither TFP-(0.1)SBC nor TFP-(0.3)SBC particles caused any notable cell death. TFP-based NPs were thus confirmed to be cytocompatible against AT1 cells up to $500 \mu\text{g/mL}$, a phenomenon previously observed with human dermal fibroblasts and normal prostate epithelial cells (PZ-HPV-7) after a similar 24 h incubation (23, 26). This is likely a result of

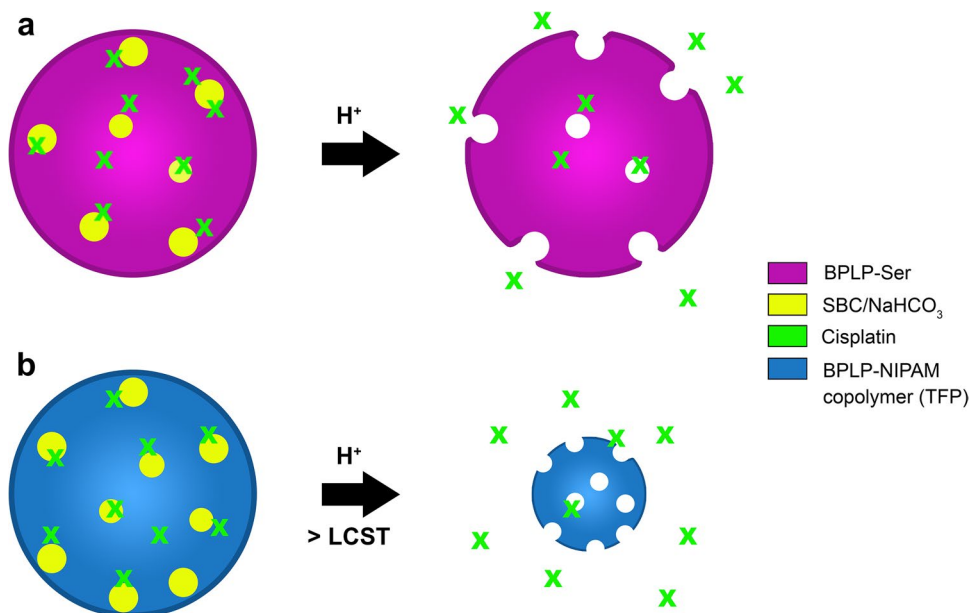
the incorporation of the cytocompatible PNIPAm within the formulation (43, 46).

Drug Loading and Release

The release profiles of the nanoformulations were expected to be dependent on the amount of SBC in each formulation. In both BPLP and TFP, the increase in available H^+ facilitates the generation of pores in the nanoparticle structure as a result of the double displacement reaction between the two. In the case of TFP, an increase in temperature beyond the LCST of the polymer also causes the nanoparticle to shrink. Both phenomena (outlined in Fig. 7) induce entrapped drugs to be ejected from the interior of the matrix; the ability of both nanoformulations to conform to these projected behaviors is therefore vital. Thus, drug release in various pH and temperature conditions was assessed.

The loading efficiency of cis-BPLP-(0.1)SBC particles was calculated to be 66%, while that of the (0.3)SBC NPs was 75%. The release profiles of both cis-BPLP-(0.1)SBC and cis-BPLP-(0.3)SBC NPs (Fig. 8a) were highly dependent upon the amount of SBC in each formulation, in turn relying on the pH of the environment. Both had near-identical, slow drug release at pH 7.4, with complete release yet to be achieved at day 14. The (0.1)SBC formulation had a rapid initial release (up to 60% cumulative release by day 2, nearly double that of both formulations at the neutral pH), followed by a slower release profile reaching approximately 91% cumulative release by day 14 at the acidic pH. BPLP-(0.3)SBC displayed the most marked change in release profile in response to a drop in pH: at pH 6.0, the formulation released 100% of loaded cisplatin by day 14, foregoing the plateaued release period observed in the other test groups between

Fig. 7 Schematics of (a) BPLP-SBC with pH- and (b) TFP-SBC NPs with pH- and temperature-responsive release characteristics.



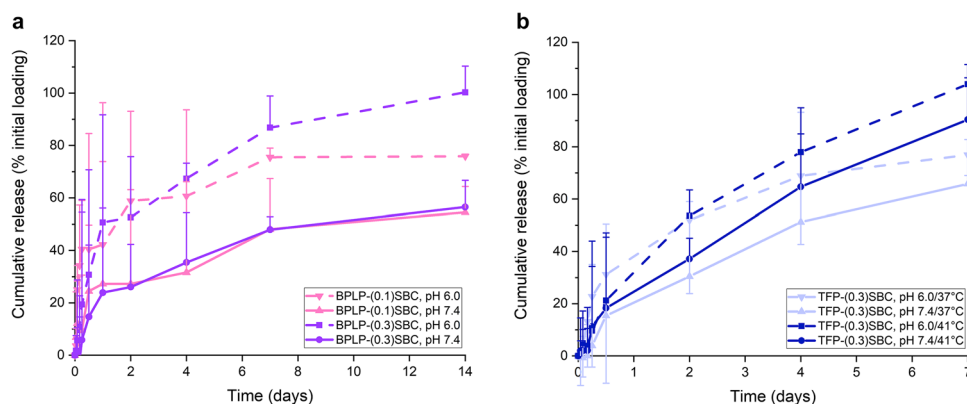


Fig. 8 Cumulative release of loaded/encapsulated cisplatin from (a) cis-BPLP-SBC NPs and (b) cis-TFP-SBC NPs at different temperatures (37 and 41°C) and pH (6.0 and 7.4) conditions. BPLP release studies showed clearly elevated release at pH 6.0 in the formulation with 30 mg of SBC, which showed near-complete release of cisplatin within 14 days. TFP release studies showed total (or near-total) release of encapsulated drug by day 4 at either pH tested at the elevated temperature; studies were discontinued after day 7 since the expected result of 100% release was achieved. (n=4 for all groups).

days 7 and 14. In contrast to previous work that examined the release profile of encapsulants from non-porous BPLP NPs, these display a higher/quicker burst release. For instance, Jiang and colleagues observed a roughly 50% release by BPLP NPs over 3 days at pH 5.0 (47)- in comparison, the BPLP NPs synthesized here showed approximately 60% release at pH 6.0. Similarly, their functional pH-sensitive formulations showed roughly 20% release by day 3 at pH 7.4- in comparison, the BPLP NPs here show just under 30% release: a nearly 30% difference relative to their behavior at acidic conditions, but slightly higher than non-porous NPs. The role of the porogen is thus quite apparent. Additionally, the above-outlined difference in the two formulations synthesized herein at the acidic pH showed clearly the role played by increasing quantities of SBC in the formulation, while their much higher/faster release at acidic pH also stood in stark contrast to their slower/lower release at neutral pH, showing the pH-responsive qualities of both formulations, irrespective of SBC concentration. They are thus functionally capable of application as pH-responsive theranostic platforms targeting cancer.

The SBC-dependent release characteristics having been established, those of cisplatin-loaded TFP NPs synthesized with 30 mg of SBC were assessed (Fig. 8b) at two pH values (6.0 and 7.4) and two temperatures (37- and 41°C). Given that the goal of TFP-based drug delivery is to modulate local drug release with local hyperthermia (40-45°C) as a trigger (or conversely, prevent excessive release at body temperature) (48, 49), the (0.1)SBC formulation which had an LCST of only about 38°C as seen in Fig. 5 was deemed not fit for purpose, as its LCST lies too close to physiological temperature. As a result, these NPs would release an unacceptably high quantity of the drug at body temperature while in circulation prior to localization in tumor tissues. Therefore, only the cis-TFP-(0.3)SBC NPs had optimal LCST and

temperature-dependent drug release properties and were explored further in this study. The loading efficiency of cis-TFP-(0.3)SBC particles was calculated to be 87%.

Overall, the release of cisplatin from the TFP NPs was markedly more rapid than that observed in the case of the BPLP formulations. At 37°C, the NPs exhibited a sustained pattern of encapsulated drug release up to approximately 80% by day 7 (71.4% and 83.8% for pH 6.0 and pH 7.4, respectively). By contrast, the increase in temperature resulted in a much more rapid release profile, with most of the entrapped drug being released by day 4 (100% and 90.4% for pH 6.0 and 7.4, respectively). The temperature-dependent release of encapsulated agents here is markedly higher than that observed in some of our previous work, most likely as a result of the addition of a porogen. Whereas the release of doxorubicin from non-porogenic TFP NPs was observed to occur to a maximum of approximately 50% (cumulative) over 2 days at 41°C, the nanoparticles synthesized herein showed >60% release during the same time at the same conditions, while even release at 37°C was improved in the same time period, from 35- to >50% (non-porous, doxorubicin vs. current formulation) (23). The observations above confirmed two desired properties/behaviors of this formulation: it responds to acidic pH as a result of the SBC porogen (albeit less notably so than in BPLP NPs) and responds markedly differently when the temperature is raised past/close to its LCST, release increasing in both situations.

The sustained release characteristics of all three nanoformulations (BPLP in particular) tested are noteworthy. Cisplatin-PNIPAM formulations in literature have exhibited very rapid release over the course of hours (50, 51) (too short for any sustained release to be effective) or incomplete delivery (sub-50% cumulative release) over the period of several days (52, 53). Sustained release over the course of several days, coupled with the natural accumulation in tumors (viz. the

enhanced permeability and retention effect), would make the application of these formulations (purely by considerations of drug delivery) better by comparison, particularly given the complete (100%) release. Dosing would be needed more infrequently, and the tumor would be consistently exposed to the drug over an extended period, possibly enhancing efficacy.

Cellular Uptake and Uptake Imaging

The results of BPLP-(0.3)SBC NP uptake by A549 cells are presented in Fig. 9. The (0.3)SBC formulation was chosen for further analysis based on the results of the release study, which showed that its release profile was the most markedly different at pH 6.0. The NPs showed a dose-dependent increase in uptake, with the most notable increase taking place at 200 $\mu\text{g/mL}$, where the fluorescence of the NPs is

>2.5x that observed at half this concentration (compared to the 2x increase observed when NP concentration is increased from 50- to 100 $\mu\text{g/mL}$).

The TFP-(0.3)SBC formulation too displayed a clearly dose-dependent increase in uptake (Fig. 10). The increase in fluorescence between 50- and 100 $\mu\text{g/mL}$ was roughly 5x, but this dropped to <2x between 100- and 200 $\mu\text{g/mL}$.

Further uptake data (based on directly-measured fluorescence of both BPLP- and TFP-(0.3)SBC NPs normalized by cell protein content) can be found in the Supporting Information (Fig. S4).

Assessment of *In Vitro* Therapeutic Efficacy

To confirm the results of the release and uptake studies and establish therapeutic efficacy *in vitro*, an anti-A549 cytotoxicity assay was carried out with both chosen BPLP- and TFP

Fig. 9 Cellular uptake of BPLP-(0.3)SBC NPs by A549 cells following 2 h incubation with increasing concentrations of NPs. (a) Brightfield (top) and fluorescent (bottom) microscopy of cells subjected to uptake; (b) quantitative data, measured as fluorescence intensity from fluorescent microscopy images.

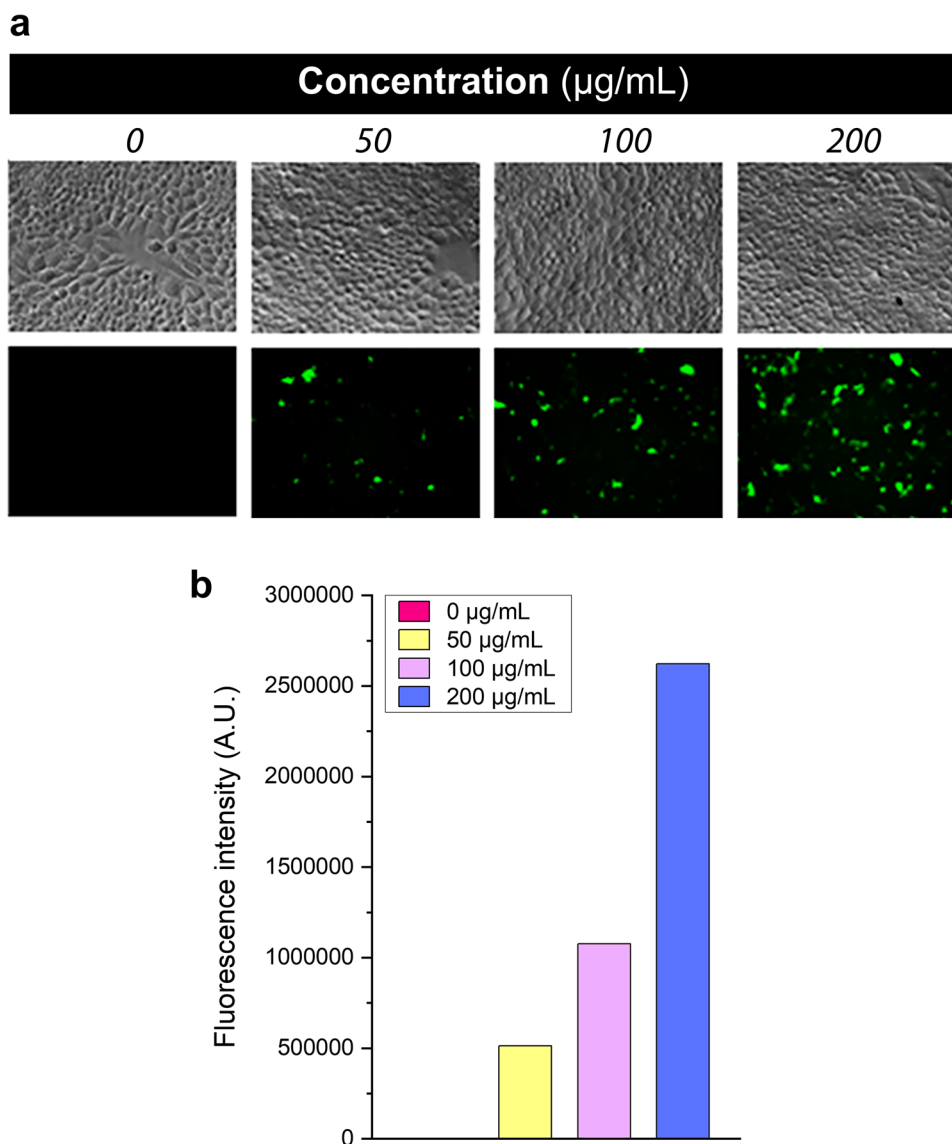
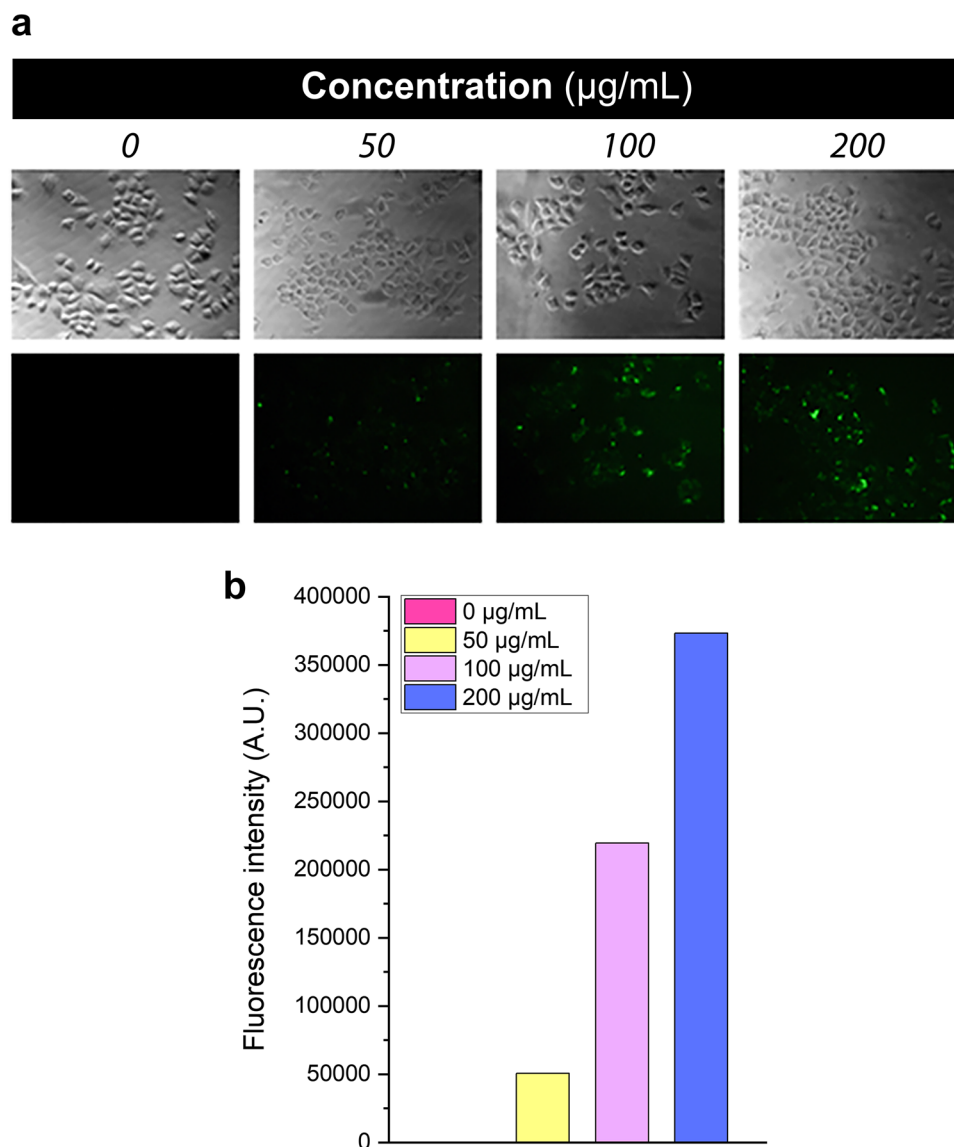


Fig. 10 Cellular uptake of TFP-(0.3)SBC NPs by A549 cells following 2 h incubation with increasing concentrations of NPs. **(a)** Brightfield (top) and fluorescent (bottom) microscopy of cells subjected to uptake; **(b)** quantitative data, measured as fluorescence intensity from fluorescent microscopy images.



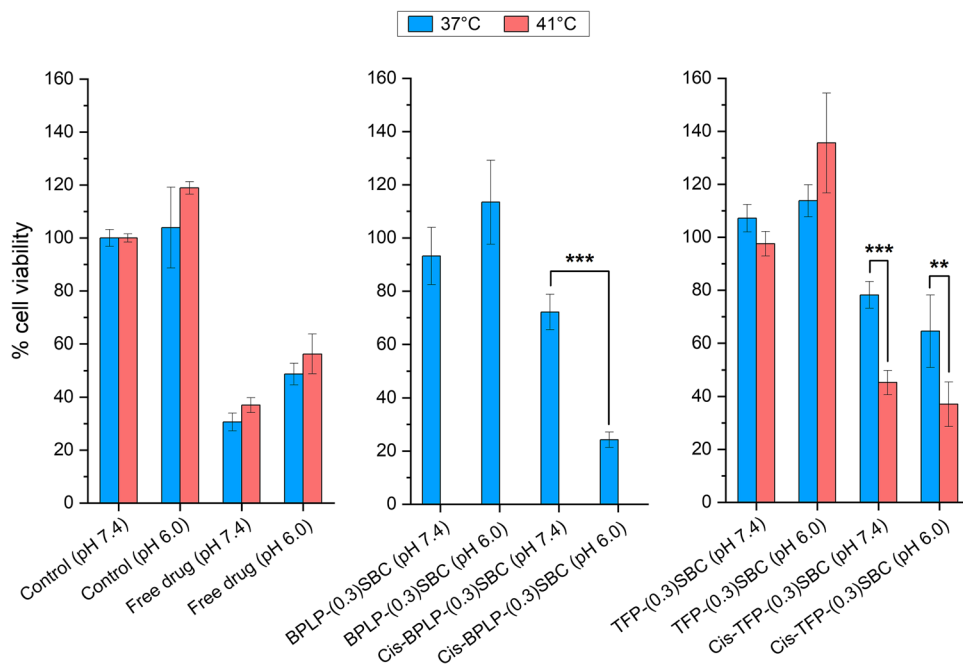
NP formulations over 4 h, with concentrations informed by the IC₅₀ of cisplatin on the cell line. The viability of cells (at both temperatures) at pH 7.4 was taken as 100% and all other data was handled with respect to these. These results are presented in Fig. 11.

As expected, the bare BPLP-(0.3)SBC NPs precipitated almost no cell death at either pH value it was tested at against the A549 cells, but cisplatin-loaded NPs showed a remarkable and statistically significant ($p \leq 0.001$) induction of cell death when the pH was decreased from 7.4 to 6.0, with cell viability decreasing from 72- to 24%.

TFP-(0.3)SBC NPs were non-toxic at both pH and temperature conditions tested but showed statistically significant decreases in viability when the temperature was increased from 37 to 41 °C, at both pH values tested, with viability

dropping from 78- to 45% at pH 7.4 and 64- to 37% at pH 6.0. Conversely—from a pH standpoint—the viability of A549 cells decreased from 78- to 64% when the pH was lowered to 6.0 at 37 °C, and from 45- to 37% when the pH was lowered to 6.0 at 41 °C. Our results thus confirm that both formulations exhibited dynamic and stimuli-responsive anticancer activity as a function of pH. The temperature also played a role in cancer cell killing in the case of the TFP-SBC NPs. Given the less-than-ideal performance of the NPs at neutral pH (i.e.-reduction in cell viability to 80% or less; corroborated by data in Fig. 8), future work could examine additives (materials that may include those such as the acid-reactive chitosan) that reinforce the NPs' inherent pH-responsive nature, preventing drug release at neutral pH and maintaining the same release as shown in Fig. 11 at acidic pH.

Fig. 11 Cancer cell killing data (relative to control) for bare nanoparticles (BPLP- or TFP-(0.3)SBC) and cisplatin-loaded particles on A549 cells. BPLP nanoparticles showed a statistically significant difference between neutral and acidic pH. TFP nanoparticles showed a statistically significant difference between 37 and 41 °C at both pH conditions. (n = 3 for all groups; ** p ≤ 0.01, *** p ≤ 0.001).



Conclusions

We report here the successful synthesis, optimization, and characterization of two distinct theranostic nanoparticle formulations with cisplatin as the active anticancer encapsulant. BPLP nanoparticles with 0.3 M sodium bicarbonate (BPLP-(0.3)SBC NPs) were identified as the most optimal of the pH-responsive nanoparticle formulations tested. The NPs were cytocompatible with the potential for sustained drug release up to 14 days, dose-dependent uptake by A549 cancer cells, and marked anticancer efficacy within the acidic environment of cancer cells. These BPLP-(0.3)SBC NPs were thus identified to be viable passively-targeted pH-responsive theranostic particles for anti-cancer drug delivery.

TFP nanoparticles with 0.3 M sodium bicarbonate (TFP-(0.3)SBC NPs) were identified as the most optimal of the dual-stimuli responsive (thermal and pH) formulations tested, showing all the desired characteristics as its BPLP counterpart and marked increases in cytocompatibility and anticancer efficacy at elevated temperatures. This formulation is thus both a minor improvement on the BPLP-based NPs (slowing down drug release at body temperature and thus slightly extending the duration of release) and a viable candidate for a theranostic platform with heat- and pH-triggered drug release properties.

Supplementary Information The online version contains supplementary material available at <https://doi.org/10.1007/s11095-022-03317-8>.

ACKNOWLEDGMENTS AND DISCLOSURES Graphical abstract created with biorender.com. The authors declare no conflicting interests

Funding This work was supported by National Institute on Alcohol Abuse and Alcoholism (NIAAA) award R21AA029750-01 and Rhode Island Foundation Medical Research Grant #20174376 (JUM). This work was also partly supported by CPRIT award RP210206 (KTN) and a National Institute of Arthritis and Musculoskeletal and Skin Diseases (NIAMS) award (AR072731) (JY).

References

- Ahmad FB, Anderson RN. The leading causes of death in the US for 2020. *JAMA* [Internet] 2021 May 11;325(18):1829–1830. Available from: <https://jamanetwork.com/journals/jama/fullarticle/2778234>
- Toale KM, Johnson TN, Ma MQ. Chemotherapy-induced toxicities. In: Todd KH, Charles R, Thomas J, Bernstein SL, Quest TE, Yeung S-CJ, editors. *Oncologic emergency medicine*. New York: Springer International Publishing; 2016. p. 381–406.
- McCarthy DM. Pain management. In: Todd KH, Charles R, Thomas J, Bernstein SL, Quest TE, Yeung S-CJ, editors. *Oncologic emergency medicine*. New York: Springer International Publishing; 2016. p. 445–54.
- Ullah MF. Cancer multidrug resistance (MDR): a major impediment to effective chemotherapy. *Asian Pac J Cancer Prev* [Internet]. 2008;9(1):1–6. Available from: <http://www.ncbi.nlm.nih.gov/pubmed/18439063>.
- Al Tameemi W, Dale TP, Al-Jumaily RMK, Forsyth NR. Hypoxia-modified cancer cell metabolism. *Front Cell Dev Biol* [Internet]. 2019. p. 7. Available from: <https://www.frontiersin.org/articles/10.3389/fcell.2019.00004/full>.
- Justus CR, Dong L, Yang LV. Acidic tumor microenvironment and pH-sensing G protein-coupled receptors. *Front Physiol* [Internet].

2013. p. 4. Available from: <https://doi.org/10.3389/fphys.2013.00354/full>.
7. Zhao B-X, Zhao Y, Huang Y, Luo L-M, Song P, Wang X, *et al.* The efficiency of tumor-specific pH-responsive peptide-modified polymeric micelles containing paclitaxel. *Biomaterials* [Internet]. 2012 Mar;33(8):2508–2520. Available from: <https://linkinghub.elsevier.com/retrieve/pii/S0142961211014323>
 8. Kim JH, Li Y, Kim MS, Kang SW, Jeong JH, Lee DS. Synthesis and evaluation of biotin-conjugated pH-responsive polymeric micelles as drug carriers. *Int J Pharm* [Internet]. 2012 May;427(2):435–442. Available from: <https://linkinghub.elsevier.com/retrieve/pii/S0378517312000683>
 9. Palanikumar L, Al-Hosani S, Kalmouni M, Nguyen VP, Ali L, Pasricha R, *et al.* pH-responsive high stability polymeric nanoparticles for targeted delivery of anticancer therapeutics. *Commun Biol* [Internet]. 2020 Dec 3;3(1):95. Available from: <http://www.nature.com/articles/s42003-020-0817-4>
 10. Prabhakar U, Maeda H, Jain RK, Sevick-Muraca EM, Zamboni W, Farokhzad OC, *et al.* Challenges and key considerations of the enhanced permeability and retention effect for nanomedicine drug delivery in oncology. *Cancer Res* [Internet] 2013 Apr 15;73(8):2412–2417. Available from: <http://cancerres.aacrjournals.org/lookup/doi/10.1158/0008-5472.CAN-12-4561>
 11. Chu S, Shi X, Tian Y, Gao F. pH-Responsive polymer nanomaterials for tumor therapy. *Front Oncol* [Internet]. 2022. p. 12. Available from: <https://doi.org/10.3389/fonc.2022.855019/full>.
 12. Mu Y, Gong L, Peng T, Yao J, Lin Z. Advances in pH-responsive drug delivery systems. *OpenNano* [Internet]. 2021 Dec;5:100031. Available from: <https://linkinghub.elsevier.com/retrieve/pii/S2352952021000013>
 13. Menon JU, Jadeja P, Tambe P, Vu K, Yuan B, Nguyen KT. Nanomaterials for photo-based diagnostic and therapeutic applications. *Theranostics* [Internet] 2013;3(3):152–166. Available from: <http://www.thno.org/v03p0152.htm>
 14. Ito A, Shinkai M, Honda H, Kobayashi T. Medical application of functionalized magnetic nanoparticles. *J Biosci Bioeng* [Internet] 2005 Jul;100(1):1–11. Available from: <https://linkinghub.elsevier.com/retrieve/pii/S1389172305704229>
 15. Zhou M, Ghosh I. Quantum dots and peptides: a bright future together. *Biopolymers* [Internet] 2007;88(3):325–339. Available from: <http://doi.wiley.com/10.1002/bip.20655>
 16. Singh N, Jenkins GJS, Asadi R, Doak SH. Potential toxicity of superparamagnetic iron oxide nanoparticles (SPION). *Nano Rev* [Internet]. 2010 Jan 1;1(1):5358. Available from: <https://www.tandfonline.com/doi/full/10.3402/nano.v1i0.5358>
 17. Stan MS, Memet I, Sima C, Popescu T, Teodorescu VS, Hermenean A, *et al.* Si/SiO₂ quantum dots cause cytotoxicity in lung cells through redox homeostasis imbalance. *Chem Biol Interact* [Internet] 2014 Sep;220:102–115. Available from: <https://linkinghub.elsevier.com/retrieve/pii/S0009279714001999>
 18. Wang ZG, Zhou R, Jiang D, Song JE, Xu Q, Si J, *et al.* Toxicity of Graphene Quantum Dots in Zebrafish Embryo. *Biomed Environ Sci* [Internet]. 2015 May;28(5):341–51. Available from: <http://www.ncbi.nlm.nih.gov/pubmed/26055561>.
 19. Mérian J, Gravier J, Navarro F, Texier I. Fluorescent nanoprobe dedicated to in vivo imaging: from preclinical validations to clinical translation. *Molecules* [Internet] 2012 May 10;17(5):5564–5591. Available from: <http://www.mdpi.com/1420-3049/17/5/5564>
 20. Alexis F, Pridgen E, Molnar LK, Farokhzad OC. Factors affecting the clearance and biodistribution of polymeric nanoparticles. *Mol Pharm* [Internet] 2008 Aug 1;5(4):505–515. Available from: <https://pubs.acs.org/doi/10.1021/mp800051m>
 21. Yang J, Zhang Y, Gautam S, Liu L, Dey J, Chen W, *et al.* Development of aliphatic biodegradable photoluminescent polymers. *Proc Natl Acad Sci* [Internet]. 2009 Jun 23;106(25):10086–10091. Available from: <https://pnas.org/doi/full/10.1073/pnas.090004106>
 22. Kuriakose AE, Pandey N, Shan D, Banerjee S, Yang J, Nguyen KT. Characterization of photoluminescent polylactone-based nanoparticles for their applications in cardiovascular diseases. *Front Bioeng Biotechnol* [Internet]. 2019. p. 7. Available from: <https://www.frontiersin.org/articles/10.3389/fbioe.2019.00353/full>.
 23. Pandey N, Menon JU, Takahashi M, Hsieh J-T, Yang J, Nguyen KT, *et al.* Thermo-responsive fluorescent nanoparticles for multimodal imaging and treatment of cancers. *Nanotheranostics* [Internet] 2020;4(1):1–13. Available from: <http://www.ntno.org/v04p001.htm>
 24. Lustberg MB, Edelman MJ. Optimal duration of chemotherapy in advanced non-small cell lung cancer. *Curr Treat Options Oncol* [Internet] 2007 Aug 9;8(1):38–46. Available from: <http://link.springer.com/10.1007/s11864-007-0020-6>
 25. Xie Z, Kim JP, Cai Q, Zhang Y, Guo J, Dhami RS, *et al.* Synthesis and characterization of citrate-based fluorescent small molecules and biodegradable polymers. *Acta Biomater* [Internet]. 2017 Mar;50:361–9. Available from: <https://linkinghub.elsevier.com/retrieve/pii/S1742706117300193>
 26. Wadajkar AS, Kadapure T, Zhang Y, Cui W, Nguyen KT, Yang J. Dual-imaging enabled Cancer-targeting nanoparticles. *Adv Healthc Mater* [Internet] 2012 Jul;1(4):450–456. Available from: <http://doi.wiley.com/10.1002/adhm.201100055>
 27. Menon JU, Jadeja P, Tambe P, Thakore D, Zhang S, Takahashi M, *et al.* Polymeric nanoparticles as dual-imaging probes for cancer management. *Biomater Biomech Bioeng*. 2016;3(3):129–40
 28. Sundaresan V, Menon JU, Rahimi M, Nguyen KT, Wadajkar AS. Dual-responsive polymer-coated iron oxide nanoparticles for drug delivery and imaging applications. *Int J Pharm* [Internet] 2014 May;466(1–2):1–7. Available from: <https://linkinghub.elsevier.com/retrieve/pii/S0378517314001598>
 29. Yadavalli T, Ramasamy S, Chandrasekaran G, Michael I, Therese HA, Chennakesavulu R. Dual responsive PNIPAM–chitosan targeted magnetic nanoparticles for targeted drug delivery. *J Magn Magn Mater* [Internet]. 2015 Apr;380:315–20. Available from: <https://linkinghub.elsevier.com/retrieve/pii/S0304885314008579>
 30. Menon JU, Kuriakose A, Iyer R, Hernandez E, Gandee L, Zhang S, *et al.* Dual-Drug Containing Core-Shell Nanoparticles for Lung Cancer Therapy. *Sci Rep* [Internet]. 2017 Dec 16;7(1):13249. Available from: <http://www.nature.com/articles/s41598-017-13320-4>
 31. Ke C-J, Chiang W-L, Liao Z-X, Chen H-L, Lai P-S, Sun J-S, *et al.* Real-time visualization of pH-responsive PLGA hollow particles containing a gas-generating agent targeted for acidic organelles for overcoming multi-drug resistance. *Biomaterials* [Internet]. 2013 Jan;34(1):1–10. Available from: <https://linkinghub.elsevier.com/retrieve/pii/S0142961212010277>
 32. Schneider CA, Rasband WS, Eliceiri KW. NIH image to ImageJ: 25 years of image analysis. *Nat Methods* [Internet] 2012 Jul 28;9(7):671–675. Available from: <http://www.nature.com/articles/nmeth.2089>
 33. Zhang P, Gao WYG, Turner S, Ducatman BS. Gleevec (STI-571) inhibits lung cancer cell growth (A549) and potentiates the cisplatin effect in vitro. *Mol Cancer*. 2003 p. 2. Available from: <https://doi.org/10.1186/1476-4598-2-1>.
 34. Ilyas A, Islam M, Asghar W, Menon JU, Wadajkar AS, Nguyen KT, *et al.* Salt-leaching synthesis of porous PLGA nanoparticles. *IEEE Trans Nanotechnol* [Internet] 2013 Nov;12(6):1082–1088. Available from: <http://ieeexplore.ieee.org/document/6585800/>
 35. Xie Z, Su Y, Kim GB, Selvi E, Ma C, Aragon-Sanabria V, *et al.* Immune Cell-Mediated Biodegradable Theranostic Nanoparticles for Melanoma Targeting and Drug Delivery. *Small* [Internet]. 2017 Mar 27;13(10):1603121. Available from: <https://onlinelibrary.wiley.com/doi/10.1002/smll.201603121>

36. Kuriakose AE, Hu W, Nguyen KT, Menon JU. Scaffold-based lung tumor culture on porous PLGA microparticle substrates. Cordes N, editor. PLoS One [Internet]. 2019 May 31;14(5). Available from: <https://dx.plos.org/10.1371/journal.pone.0217640>
37. Zhao G, Ishizaka T, Kasai H, Oikawa H, Nakanishi H. Fabrication of unique porous polyimide nanoparticles using a Reprecipitation method. Chem Mater [Internet] 2007 Apr 1;19(8):1901–1905. Available from: <https://pubs.acs.org/doi/10.1021/cm062709w>
38. Chung HJ, Kim HK, Yoon JJ, Park TG. Heparin immobilized porous PLGA microspheres for Angiogenic growth factor delivery. Pharm Res [Internet] 2006 Aug 21;23(8):1835–1841. Available from: <http://link.springer.com/10.1007/s11095-006-9039-9>
39. Oh YJ, Lee J, Seo JY, Rhim T, Kim S-H, Yoon HJ, *et al.* Preparation of budesonide-loaded porous PLGA microparticles and their therapeutic efficacy in a murine asthma model. J Control Release [Internet] 2011 Feb 28;150(1):56–62. Available from: <https://linkinghub.elsevier.com/retrieve/pii/S0168365910008990>
40. Cai W, Gupta RB. Thermosensitive and ampholytic hydrogels for salt solution. J Appl Polym Sci [Internet] 2003 May 23;88(8):2032–2037. Available from: <http://doi.wiley.com/10.1002/app.11910>
41. Shekhar S, Mukherjee M, Sen AK. Studies on thermal and swelling properties of poly (NIPAM-co-2-HEA) based hydrogels. Adv Mater Res [Internet] 2012 Dec 25;1(4):269–284. Available from: <http://koreascience.or.kr/journal/view.jsp?kj=TPTPLG&py=2012&vnc=v1n4&sp=269>
42. Pei Y, Chen J, Yang L, Shi L, Tao Q, Hui B, *et al.* The effect of pH on the LCST of poly(N-isopropylacrylamide) and poly(N-isopropylacrylamide-co-acrylic acid). J Biomater Sci Polym Ed [Internet] 2004 Jan 2;15(5):585–594. Available from: <https://www.tandfonline.com/doi/full/10.1163/156856204323046852>
43. Dhamecha D, Le D, Chakravarty T, Perera K, Dutta A, Menon JU. Fabrication of PNIPAm-based thermoresponsive hydrogel microwell arrays for tumor spheroid formation. Mater Sci Eng C [Internet]. 2021 Jun;125:112100. Available from: <https://linkinghub.elsevier.com/retrieve/pii/S0928493121002393>
44. Wang J, Wang S, Manzer R, McConville G, Mason RJ. Ozone induces oxidative stress in rat alveolar type II and type I-like cells. Free Radic Biol Med [Internet] 2006 Jun;40(11):1914–1928. Available from: <https://linkinghub.elsevier.com/retrieve/pii/S089158490600061X>
45. Mason RJ. Biology of alveolar type II cells. Theatr Res Int. 2006 Jan;11(s1):S12–5 Available from: <https://onlinelibrary.wiley.com/doi/10.1111/j.1440-1843.2006.00800.x>.
46. Cooperstein MA, Canavan HE. Assessment of cytotoxicity of (N-isopropyl acrylamide) and Poly(N-isopropyl acrylamide)-coated surfaces. Biointerphases [Internet]. 2013 Dec;8(1):19. Available from: <http://avs.scitation.org/doi/10.1186/1559-4106-8-19>
47. Jiang Z, Tian Y, Shan D, Wang Y, Gerhard E, Xia J, *et al.* pH protective Y1 receptor ligand functionalized antiphagocytosis BPLP-WPU micelles for enhanced tumor imaging and therapy with prolonged survival time. Biomaterials [Internet]. 2018 Jul;170:70–81. Available from: <https://linkinghub.elsevier.com/retrieve/pii/S0142961218302424>
48. Suit HD, Shwayder M. Hyperthermia: potential as an anti-tumor agent. Cancer [Internet] 1974;34(1):122–129. Available from: [https://doi.org/10.1002/1097-0142\(197407\)34:1%3C122::AID-CNCR2820340118%3E3.0.CO;2-R](https://doi.org/10.1002/1097-0142(197407)34:1%3C122::AID-CNCR2820340118%3E3.0.CO;2-R)
49. Pradhan P, Jaiswal MK, Gogoi M, Bahadur D, Banerjee R. Magnetic nanoparticles and thermosensitive carriers for hyperthermia and drug delivery. In: Banerjee R, editor. Nanotechnology: diagnosis and treatment of cancers. New Delhi: Narosa Publishing House; 2011.
50. Fang J-Y, Chen J-P, Leu Y-L, Hu J-W. The delivery of platinum drugs from thermosensitive hydrogels containing different ratios of chitosan. Drug Deliv [Internet] 2008 Jan 10;15(4):235–243. Available from: <http://www.tandfonline.com/doi/full/10.1080/10717540802006674>
51. Chen J-P, Leu Y-L, Fang C-L, Chen C-H, Fang J-Y. Thermosensitive hydrogels composed of hyaluronic acid and gelatin as carriers for the Intravesical Administration of Cisplatin. J Pharm Sci [Internet] 2011 Feb;100(2):655–666. Available from: <https://linkinghub.elsevier.com/retrieve/pii/S002235491532308X>
52. Cheng C, Xia D, Zhang X, Chen L, Zhang Q. Biocompatible poly(N-isopropylacrylamide)-g-carboxymethyl chitosan hydrogels as carriers for sustained release of cisplatin. J Mater Sci [Internet] 2015 Jul 28;50(14):4914–4925. Available from: <http://link.springer.com/10.1007/s10853-015-9036-7>
53. Salimi F, Dilmaghani KA, Alizadeh E, Akbarzadeh A, Davaran S. Enhancing cisplatin delivery to hepatocellular carcinoma HepG2 cells using dual sensitive smart nanocomposite. Artif Cells, Nanomedicine, Biotechnol [Internet]. 2018 Jul 4;46(5):949–58. Available from: <https://www.tandfonline.com/doi/full/10.1080/21691401.2017.1349777>

Publisher's Note Springer Nature remains neutral with regard to jurisdictional claims in published maps and institutional affiliations.